MOLECULAR AND CELLULAR BIOLOGY, July 2005, p. 5699–5711 Vol. 25, No. 13
0270-7306/05/$08.00+0 doi:10.1128/MCB.25.13.5699–5711.2005

Transcription Factor KLF7 Is Important for Neuronal Morphogenesis in Selected Regions of the Nervous System

Friedrich Laub,[1,2] Lei Lei,[3] Hideaki Sumiyoshi,[1]† Daisuke Kajimura,[1] Cecilia Dragomir,[1] Silvia Smaldone,[1,2] Adam C. Puche,[4] Timothy J. Petros,[5] Carol Mason,[5,6] Luis F. Parada,[3] and Francesco Ramirez[1,2]*

Laboratory of Genetics and Organogenesis, Research Division of the Hospital for Special Surgery, and Department of Physiology and Biophysics at Weill Medical College of Cornell University, 535 East 70th Street, New York, New York 10021[1]; CEINGE-Biotecnologie Avanzate, 80131 Naples, Italy[2]; Center for Developmental Biology and Kent Waldrep Center for Nerve Growth and Regeneration, University of Texas Southwestern Medical Center, 6000 Harry Hines Blvd., Dallas, Texas 75390-9133[3]; Department of Anatomy and Neurobiology, School of Medicine, University of Maryland, 20 Penn St., Baltimore, Maryland 21201[4]; and Center for Neurobiology and Behavior[5] and Department of Pathology,[6] Columbia University, 630 West 168th Street, New York, New York 10032

Received 30 December 2004/Returned for modification 12 March 2005/Accepted 7 April 2005

The Krüppel-like transcription factors (KLFs) are important regulators of cell proliferation and differentiation in several different organ systems. The mouse *Klf7* gene is strongly active in postmitotic neuroblasts of the developing nervous system, and the corresponding protein stimulates transcription of the cyclin-dependent kinase inhibitor *p21$^{waf/cip}$* gene. Here we report that loss of KLF7 activity in mice leads to neonatal lethality and a complex phenotype which is associated with deficits in neurite outgrowth and axonal misprojection at selected anatomical locations of the nervous system. Affected axon pathways include those of the olfactory and visual systems, the cerebral cortex, and the hippocampus. In situ hybridizations and immunoblots correlated loss of KLF7 activity in the olfactory epithelium with significant downregulation of the *p21$^{waf/cip}$* and *p27^{kip1}* genes. Cotransfection experiments extended the last finding by documenting KLF7's ability to transactivate a reporter gene construct driven by the proximal promoter of *p27^{kip1}*. Consistent with emerging evidence for a role of Cip/Kip proteins in cytoskeletal dynamics, we also documented p21$^{waf/cip}$ and p27^{kip1} accumulation in the cytoplasm of differentiating olfactory sensory neurons. KLF7 activity might therefore control neuronal morphogenesis in part by optimizing the levels of molecules that promote axon outgrowth.

Gene-targeted deletions in mice have demonstrated that members of the mammalian family of C_2H_2 zinc finger Krüppel-like factors (KLFs) play important roles in cell differentiation and embryonic development (5, 10, 26). These functions include control of erythroid cell proliferation and β-*globin* gene cluster activity (KLF1) (8, 45, 48); regulation of lung formation, blood vessel stabilization, and T-cell quiescence (KLF2) (30, 31, 61); terminal differentiation of dermal and intestinal epithelia (KLF4) (28, 53); involvement in cardiovascular remodeling (KLF5) (54); and modulation of uterine function (KLF9) (55). Additionally, KLF6 has been reported to be a tumor suppressor protein in prostate and colon cancers (44). KLF-like gene products have been also identified in lower vertebrate and invertebrate organisms, in which they appear to control cell differentiation during embryonic development (11, 24, 29, 46). Mammalian KLFs and the closely related group of Sp1-like proteins comprise 21 distinct molecules, which display highly homologous carboxy-terminal DNA-binding sequences and divergent amino-terminal domains that regulate gene transcription (5, 10, 26). KLF/Sp1-like proteins bind to similar "GT-box or CACCC element" sites on DNA and can function as activators, repressors, or both, depending on the promoter and cellular contexts (5, 10, 26).

KLF7 was originally identified during a PCR-based search of novel KLF transcripts and found to be broadly expressed at low levels in adult tissues, hence the early name of UKLF, for ubiquitous KLF (39). Subsequent gene expression studies of the developing mouse revealed that accumulation of *Klf7* transcript is restricted to postmitotic neuroblasts of the developing central (CNS) and peripheral nervous systems (32, 35). Examples include the differentiating neuroblasts in the spinal cord, dorsal root ganglia (DRG), sympathetic ganglia, cerebral and cerebellar cortexes, hippocampus, olfactory system, and retina. Postnatal *Klf7* expression was instead found to remain constitutively high only in the DRG, cerebellum, and olfactory system. Very recent studies demonstrated that KLF7 binds to and stimulates the activity of the proximal promoter of the cyclin-dependent kinase (cdk) inhibitor *p21$^{waf/cip}$* gene (56). Based on these lines of correlative evidence, we proposed that KLF7 may be part of the genetic programs that regulate differentiation of progenitor cells, neuronal morphogenesis, and/or phenotype maintenance (32).

In order to elucidate the physiological function of KLF7 during mouse development, we have ablated its expression by

* Corresponding author. Mailing address: Laboratory of Genetics and Organogenesis, Research Division of the Hospital for Special Surgery, and Department of Physiology and Biophysics at Weill Medical College of Cornell University, 535 East 70th St., New York, NY 10021. Phone: (212) 774-7554. Fax: (212) 774-2301. E-mail: ramirezf@hss.edu.

† Present address: Department of Anatomy, Biology and Medicine, Oita Medical University, Oita 879-5593, Japan.

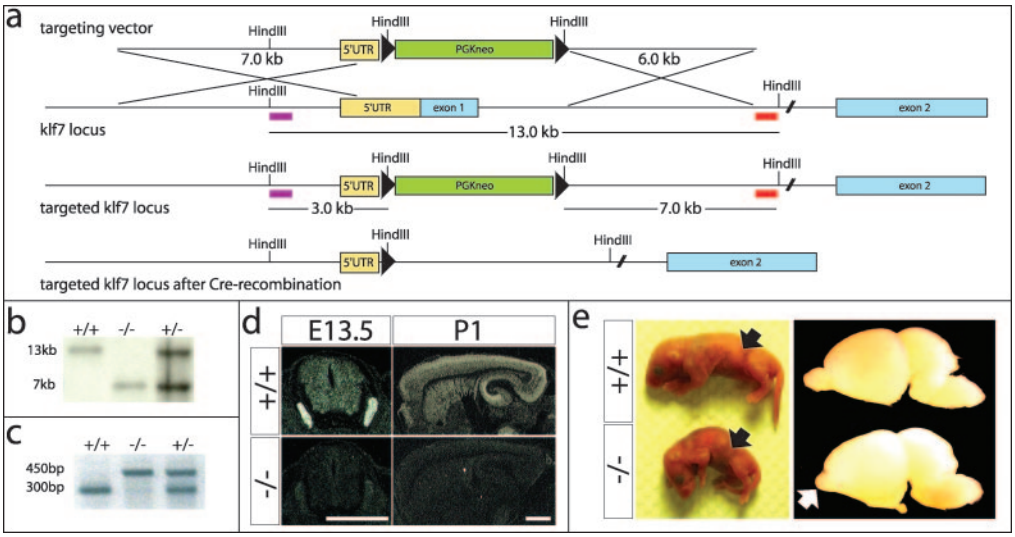

FIG. 1. *Klf7*$^{-/-}$ mice. (a) From top to bottom are shown the *Klf7* targeting construct, the wild-type locus before and after homologous recombination, and the mutant allele after Cre-mediated excision of the PGK-*neo* cassette. The black triangles indicate *loxP* sites, and the small purple and red boxes indicate the 5′ and 3′ genotyping probes, respectively, with the resulting HindIII size fragments indicated below. UTR, untranslated region. (b) Southern blot analysis of HindIII-digested genomic DNA from wild-type and heterozygous and homozygous ΔK7-*neo* mice using the 3′ probe. (c) PCR genotyping of genomic tail DNA from wild-type and heterozygous and homozygous ΔK7 mice. (d) *Klf7* in situ hybridizations of E13.5 coronal spinal cord (left) and P1 sagittal brain (right) sections from wild-type (top) and *Klf7*$^{-/-}$ mice (bottom). Hybridizations with the sense probe yielded a background signal of the same intensity as the antisense probe with the mutant tissues (data not shown). Bars, 500 μm. (e) Left side: photographs of newborns showing a *Klf7*$^{-/-}$ mouse without milk in its stomach (black arrows). Right side: photographs documenting lack of a fully formed olfactory bulb in *Klf7*$^{-/-}$ newborns (white arrow); $n = 10$ per genotype.

gene targeting in embryonic stem (ES) cells. Here we report that loss of KLF7 activity leads to impaired axon projection in the olfactory and visual systems, cerebral cortex, and hippocampus, as well as reduced dendritic branching in the hippocampus. Consistent with previous findings, we found a significant downregulation of *p21*$^{waf/cip}$ gene expression in the olfactory sensory neurons (OSNs) of *Klf7*-null mice. We also observed a similar decrease in p27^{kip1} protein levels, which was associated with KLF7's ability to transactivate the *p27*^{kip1} promoter in cell transfection assays. Finally, we present correlative evidence suggesting that p21$^{waf/cip}$ and p27^{kip1} may contribute to the neuronal morphogenesis in the olfactory epithelium (OE).

MATERIALS AND METHODS

Generation of targeted and transgenic mice. The targeting vector was designed to replace most of exon 1 with the phosphoglycerate kinase (PGK)-*neo* cassette flanked by *loxP* sites (Fig. 1). Maintenance, transfection, and selection of mouse ES cells were performed as described previously (42). Two correctly targeted ES cell clones were selected to produce *Klf7*-null mice and yielded identical phenotypes. Electroporated ES cells and mutant mice were genotyped by Southern hybridization to probes upstream and downstream of the recombination site and by PCR amplification. Amplification primers included forward primer 5′-TTTCCTGGCAGTCATCTGCAC-3′ and reverse primer 5′-GGGTC TGTTTGTTTGTCAGTCTGTC-3′ to detect exon 1 of *Klf7* and forward primer 5′-GCAGTCATCTGCACTGTACACG-3′ and reverse primer 5′-CGTTGTAA AACGACGGCCAGTG-3′ to detect the mutant allele without PGK-*neo*. About 200 ng of genomic DNA was PCR amplified for 35 cycles each under the following conditions: 95°C for 1 min, 63°C for 1 min, and 72°C for 1 min (first set of primers) and 95°C for 30 s, 60°C for 1 min, and 72°C for 30 s (second set of primers). Transgenic CMV::*Cre* mice were employed to excise the PGK-*neo* cassette in animals heterozygous for the targeted allele (42). The OMP::*eGFP* transgene included a 2-kb cassette made of the *eGFP* gene and the splice sites of the β-*globin* third intron, in addition to part of the 3′ untranslated region of the *Drosophila melanogaster Klf7* transcript in order to monitor transgene expression in mice (11). This 2-kb cassette was placed downstream of the olfactory marker protein (OMP) promoter and translational start codon (a gift of F. Margolis, Baltimore, Md.) (9). The P2:*lacZ* transgenic mouse line was a gift of P. Mombaerts (New York, N.Y.) (41). Transgenic and targeted animals were generated by standard protocols at the Mount Sinai Mouse Genetics Shared Resource Facility (New York, N.Y.) (42).

Nucleic acid and protein analyses. In situ hybridizations were performed as described previously (32); probes included *Klf7*, *Foxp1*, *Foxp2*, *Ror*β, *Reelin* (a gift from T. Curran, Memphis, Tenn.), and *p21*$^{waf/cip}$ (a gift from B. Vogelstein, Baltimore, Md.). For immunoblots, septa were isolated from four P1 mice and pooled together after removal of the airway epithelium. Antibodies against p21$^{waf/cip}$ and p27^{kip1} (1:1,000) were from Santa Cruz Biotechnology (Santa Cruz, CA), and those against TuJ (1:1,500) were from Chemicon (Temecula, CA); immunoblot assays were performed as described previously (32).

Promoter assays. Functional assays employed a luciferase reporter gene construct driven by the 2.3-kb-long *p27*^{kip1} promoter sequence (a gift from G. Sonenshein, Boston, Mass.). The reporter gene construct was cotransfected into NIH 3T3 cells together with the Myc-tagged KLF7 expression vector, and luciferase activity was evaluated using a commercial kit (Promega, Madison, WI); transfection efficiency was normalized against the constitutively expressed *Renilla* luciferase gene (56). Functional assays were performed three times in duplicate, and the statistical significance of the resulting data was determined by the Mann-Whitney U test.

ChIP assay. Chromatin immunoprecipitation (ChIP) was performed as described previously (56). 293T cells (~1×10^6) were transfected with 20 μg of Myc-tagged KLF7 expression vector or the control Myc-tagged plasmid, and ChIP was performed using a commercial kit (Upstate Biotechnology, Lake Placid, NY). Two consecutive PCRs were carried out, using 1 μl of the initial sample DNA (out of 20 μl total) and 1 μl of the first PCR mixture, respectively. Dimethyl sulfoxide was added at a final concentration of 10%. The cycling conditions were 25 cycles of 95°C for 1 min, 63°C for 1 min, and 72°C for 1 min, which was preceded by an initial denaturation step (95°C for 5 min) and a final extension step (72°C for 10 min). Amplified products were visualized by standard 2% agarose gel electrophoresis. The *p27*^{kip1} primers were forward primer 5′-A GGCCAGCCAGAGCAGGTTTGTTG-3′ and reverse primer 5′-TATGGCGG TGGAAGGGAGGCTGAC-3′.

Histological analyses. Tissue specimens were fixed in 4% paraformaldehyde; washed; decalcified in EDTA; and either infiltrated with sucrose, frozen in OCT,

and sectioned on a cryostat or dehydrated, embedded in paraffin, and sectioned on a regular microtome. Secondary antibodies were conjugated to either Alexa dyes (Molecular Probes, Eugene, OR) or biotin and then probed using the ABC procedure (Vector Labs, Burlingame, CA). Staining was visualized on a Nikon microscope using bright-field or fluorescence optics or on a Zeiss confocal laser scanning microscope. Antibodies were against OMP (a gift from F. Margolis, Baltimore, Md.); TuJ (Sigma, St. Louis, MO); TAG-1 (DSHB, Iowa City, IA); $p21^{waf/cip}$ and $p27^{kip1}$ (Santa Cruz Biotechnology, Santa Cruz, CA); and GAP43, green fluorescent protein (GFP), NCAM, L1, and phospho-histone 3 (Chemicon, Temecula, CA). Golgi-Cox staining was performed using a commercial kit (FD Neurotechnologies, Catonsville, MD).

Histomorphometric and cellular analyses. Histomorphometric and cellular analyses of the OE were performed on three coronal sections taken from comparable levels of wild-type and mutant septa along the rostro-caudal axis. Sections were subjected to phospho-histone 3 immunochemistry or TUNEL (terminal deoxynucleotidyltransferase-mediated dUTP-biotin nick end labeling) assay, and positive cells along the septum were counted using Metamorph software. To estimate cell density, nuclei were stained with DAPI (4′,6′-diamidino-2-phenylindole), imaged by Zeiss LSM510 laser scanning confocal microscopy, and counted within multiple adjacent fields. Overall OE thickness was determined by measuring the distance from the basal lamina to the apical limit of the OE at multiple points along the septum. The cortical thickness of P1 brains was determined by measuring the distance between ventricle and brain surface at its greatest extension using midsagittal sections. Cortical cell numbers in a 170-μm-wide column from the ventricle to the surface of the brain were measured using the same sections and coordinates. The number of phospho-histone 3-positive cells was determined in the ventricular part of this column. All measurements were performed with Metamorph software (Universal Imaging Corporation, Downingtown, PA). Unless otherwise indicated in the figure legends, four or more animals per genotype and time point were used for embryonic/perinatal analyses and three or more were used for adult phenotypes.

Olfactory neuron cultures and retinal axon labeling. Primary OSNs were prepared and cultured as described previously (51). Cells were fixed for 10 min in 4% paraformaldehyde, and antibodies were blocked for 30 min in 2% normal goat serum–0.2% Triton X-100; primary and secondary antibodies were incubated for 12 h at 4°C and for 1 h at room temperature, respectively. Antibody dilutions in blocking solution were 1:800 for $p21^{waf/cip}$ and 1:400 for $p27^{kip1}$. Neurons were identified based on their morphology and expression of neuronal tubulin (TuJ), using a specific antibody (1:1,000 dilution). Detection and quantification of fluorescent signals in the entire cell were performed using the Metamorph software package (Universal Imaging Corporation, Downingtown, PA). Anterograde DiI labeling of the retinal projection was performed as described previously (50). Briefly, a small DiI crystal (Molecular Probes, Eugene, OR) was placed on the optic nerve head and allowed to diffuse through the optic nerve and chiasm; heads were kept in phosphate buffer with sodium azide for ~3 weeks at 37°C. Specimens were dissected and photographed as whole mounts under a fluorescent microscope.

RESULTS

Generation of *Klf7*$^{-/-}$ mice. KLF7 activity in the developing mouse was abolished by replacing the first exon of the gene with the PGK-*neo* cassette flanked by *loxP* sites (ΔK7-*neo* allele); homozygous mutant mice without the PGK-*neo* cassette (ΔK7/ΔK7) were generated by crossing heterozygous ΔK7-*neo* animals with transgenic mice constitutively expressing Cre recombinase under the control of the cytomegalovirus promoter (Fig. 1a). Segregation of the mutant *Klf7* alleles was followed by Southern hybridization (ΔK7-*neo* allele) or PCR amplification (ΔK7 allele) (Fig. 1b and c). In situ hybridizations of E13.5 spinal cord and P1 brain to a *Klf7* probe documented loss of gene expression in homozygous ΔK7-*neo* and ΔK7 mice, respectively (Fig. 1d). This last result was independently confirmed by Northern blot hybridizations, as well as by the failure to identify shorter in-frame *Klf7* transcripts in reverse transcription-PCR or 5′ rapid amplification of cDNA end products obtained from homozygous mutant tissues (data not shown). ΔK7/ΔK7 and ΔK7-*neo*/ΔK7-*neo* mice were born at the expected Mendelian frequency and displayed the same phenotype. Specifically, the vast majority of mutant homozygotes (98.5% of a total of 800 offspring) died within the first 3 days of life, showing little or no milk in the stomachs, hypopnea, cyanosis, and failed response to clamp stimulation of their tails (Fig. 1e). Severely hypoplastic olfactory bulbs (OBs) were the only overt anatomical abnormality of *Klf7*-null mice (Fig. 1e). By contrast, ΔK7/+ or ΔK7-*neo*/+ mice displayed no anatomical abnormalities and were fertile and viable. The analyses described below were performed on ΔK7-*neo*/ΔK7-*neo* mice in the mixed genetic background 129Sv;C57BL/6.

Klf7$^{-/-}$ mice have axon outgrowth defects in the olfactory and optic nerves. The primary olfactory pathway consists of OSNs that project axons from the olfactory OE to the bulbs, where they synapse with projection neurons, which in turn relay odor information to higher brain centers (Fig. 2a) (27). Development of the olfactory nerve in the mouse begins at ~E9.5 with the emergence of OSNs in the OE and progresses with neurite formation at ~E11.5 and contact of the forebrain by ~E12.5 (6). In situ hybridizations detected high levels of *Klf7* transcripts in the OE as early as E11.5 (Fig. 2b). Immunofluorescence analyses of coronal sections of OBs from newborn (P1) *Klf7*-null mice with markers for immature (GAP43) or mature (OMP) OSNs revealed lack of peripheral innervation. However, the number of OSNs within the olfactory epithelium of mutant mice did not appear to be substantially reduced at this developmental stage (Fig. 2c and data not shown) (2). By contrast, standard histology documented a seemingly normal nasal cavity in which the olfactory nerve had crossed the cribriform plate and entered the brain cavity (Fig. 2d). Lack of peripheral innervation was further corroborated in nullizygous *Klf7* mice harboring genetically marked OSNs. These mice were generated by intercrossing *Klf7* mutant animals with transgenic animals expressing *lacZ* or enhanced GFP in a subset of or in all OE neurons under the control of the promoters of the P2 olfactory receptor or the OSN-specific OMP promoter, respectively (Fig. 2e).

Next, we followed nerve development in the olfactory cavity of mutant and wild-type mice in order to assess whether a transient contact might have been established between mutant axons and forebrain during embryogenesis. NCAM immunofluorescence, which marks axonal projections, showed that mutant neurites form at the right time (E11.5) but are fewer than in the wild-type sample; additionally, axon projections towards the forebrain are poor compared to wild-type controls (Fig. 3a). Another axonal marker, GAP43, was employed to document that, unlike the wild-type counterpart, the mutant nerve fails to contact the E12.5 forebrain and later (E17.5) remains on the inner surface of the cribriform plate (Fig. 3a). Together, this evidence favored the notion of a defect in axon growth. Parallel histomorphometric and immunohistochemical analyses failed to identify significant changes in OE thickness, cell density, proliferation, or apoptosis, thus excluding the possibility that loss of OSNs could account for the mutant phenotype (Fig. 3b). We therefore concluded that the lack of OB innervation observed in newborn *Klf7*-null mice reflects mostly the involvement of the transcription factor in regulating OSN projection.

In the absence of other overt anatomical malformations, we examined axon projections in another sensory pathway, the

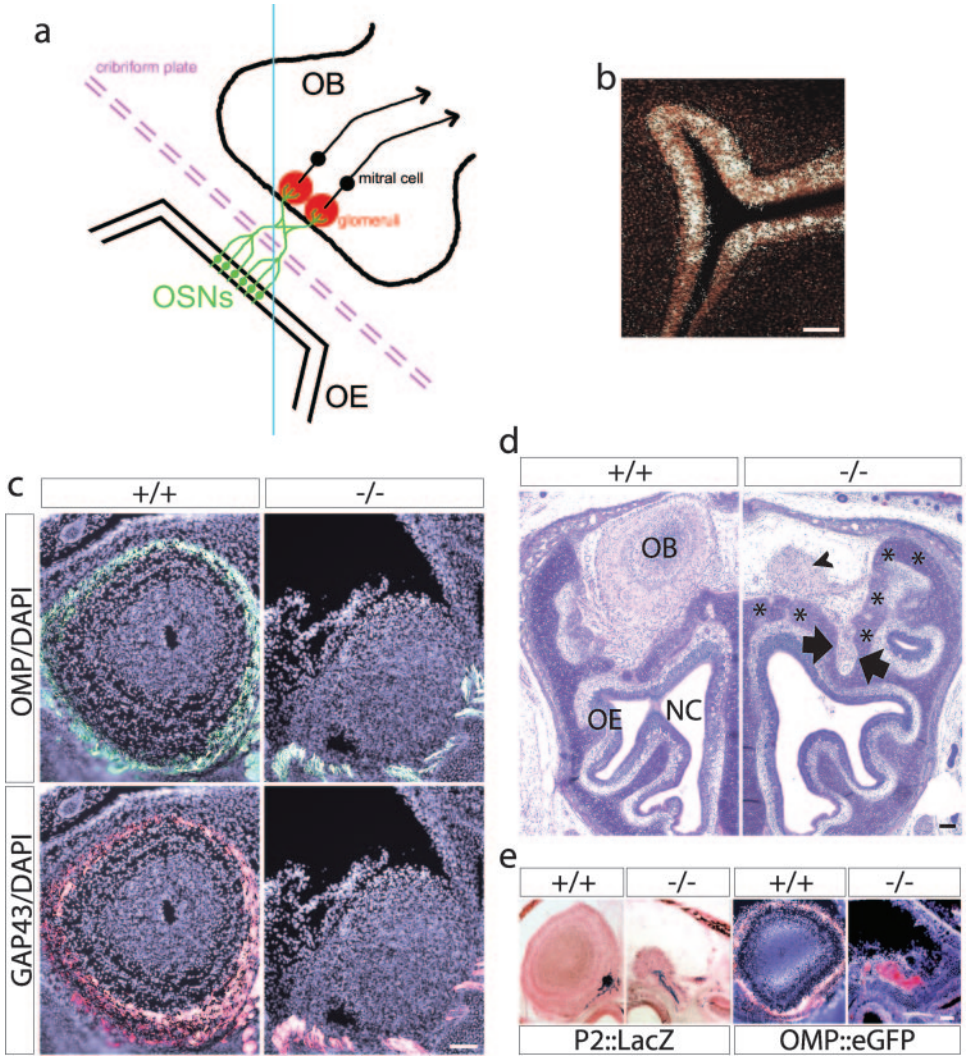

FIG. 2. Olfactory phenotype of *Klf7*$^{-/-}$ mice at P1. (a) Scheme of the mature olfactory system with the blue line indicating the plane of the sections (coronal) shown in panels c to e. Dorsal is up. (b) In situ detection of *Klf7* mRNA on a coronal section through the E11.5 OE. The signal is pseudocolored white and merged with the image of the underlying DAPI-stained tissue pseudocolored in red. (c) Sections through OBs immunostained with antibodies against OMP or GAP43 and with nuclei visualized by DAPI (n = 10 per genotype). (d) Sections of the olfactory system (farther rostral than in panel c) stained with hematoxylin and eosin. The *Klf7*$^{-/-}$ olfactory nerve (arrows) penetrates the cribriform plate (asterisks); the overall architecture of the olfactory cavity is normal, but the olfactory nerve ends in a tangle of axons (arrowhead) (n = 8 per genotype). NC, nasal cavity. (e) Genetic marking of OSNs expressing the P2 olfactory receptor (n = 1 per genotype) or the prototypical olfactory neuron marker OMP (n = 2 per genotype) in *Klf7*$^{-/-}$ mice. P2 expression is visualized by *lacZ* staining (blue), and the sections are counterstained with hematoxylin and eosin; OMP expression is visualized by anti-enhanced GFP immunofluorescence (red), and nuclei are counterstained with DAPI. Bars, 100 μm.

neonatal visual system. Retinal ganglion cell (RGC) axons exit the retina at the optic nerve head and navigate through the optic nerve to reach the optic chiasm, at which point they diverge to form ipsilateral and contralateral projections (Fig. 4a). In situ hybridization revealed that *Klf7* is highly expressed in RGCs from the time that they first emerge (~E12) through E17.5 (Fig. 4b). Initial histological analyses failed to reveal any obvious morphological differences between *Klf7*$^{-/-}$ and wild-type retinas. To visualize RGC axonal projections, we used the pan-neuronal marker GAP43. Immunofluorescence analyses revealed that mutant RGC axons project to the optic nerve head properly, but a small portion of them make aberrant projections and fail to exit the retina (Fig. 4c). These findings were substantiated with another axonal marker, TAG-1, a protein related to the L1 family of cell adhesion molecules (20). These axon guidance errors are similar to those reported in netrin-1 mutants (12). Unlike GAP43 staining, TAG-1 staining revealed a surprising difference between *Klf7*$^{-/-}$ and wild-type animals. Whereas TAG-1 labeled the entire visual pathway from retina through optic tract in wild-type embryos (Fig. 4c and d), TAG-1 expression in *Klf7*$^{-/-}$ animals was strongly decreased at the chiasm and absent in the optic tract (Fig. 4d). There is some evidence of moderately decreased TAG-1 levels in RGC axons after exit from the optic chiasm (38), but no studies have reported an absence of TAG-1 staining as seen in the *Klf7* mutants. Interestingly, we also found that TAG-1

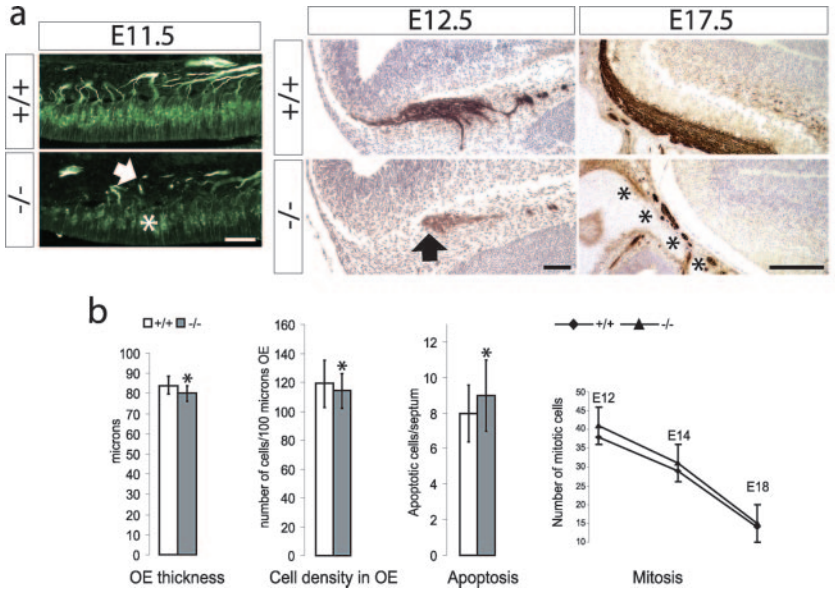

FIG. 3. Developmental progression of the olfactory phenotype in *Klf7*$^{-/-}$ embryos. (a) At left are coronal sections through the E11.5 OE stained with anti-NCAM antibodies to visualize early OSNs and their axons. The arrow and asterisk indicate reduced axon growth and number of differentiating neurons in the mutant embryo, respectively. Dorsal is right, and lateral is up. At right are sagittal sections of the E12.5 and E17.5 olfactory nerve stained with anti-GAP43 antibodies. The arrow highlights the olfactory nerve that in the mutant tissue is stalled below the forebrain instead of contacting it; the asterisks indicate the location of the cribriform plate. Rostral is left, and dorsal is up; $n = 6$ per time point and per genotype. (b) Histomorphometric and cellular features of the mutant and wild-type OE. OE thickness, cell density, and apoptosis were determined at birth, whereas the numbers of mitotic cells were evaluated at E12, E14, and E18. These numbers reflect positive cells per olfactory invagination (E12 and E14) and per one side of septum (E18). Bar graphs reflect the means ± standard deviations; *, *P* values were determined (Student's unpaired *t* test) and found not to be significant (≥0.05); $n = 4$ per time point and genotype. Bars in panel a, 50 μm (E11.5), 70 μm (E12.5), and 200 μm (E17.5).

appears to be preferentially expressed in the ventral portion of the optic tract (Fig. 4d).

Anterograde DiI labeling of RGC fibers was performed to monitor projection errors at the chiasm. Unlike the very small ipsilateral projection in wild-type heads, mutant samples displayed an increase in ipsilaterally projecting fibers (Fig. 4e). It is unknown if this new population of ipsilateral fibers arises from increased projections from the ventrotemporal retina (which normally project ipsilaterally) or ectopic projections from other regions of the retina. This point notwithstanding, we concluded that KLF7 plays an important role in RGC axon guidance at the optic nerve head and the optic chiasm and that its absence causes postchiasmatic TAG-1 expression to be downregulated.

Klf7$^{-/-}$ mice have defects of axon growth in the brain. Having demonstrated KLF7 involvement in neurite outgrowth in the olfactory and optic system, we searched for similar deficits in the *Klf7*$^{-/-}$ brain. *Klf7* is highly expressed throughout the brain during embryogenesis and soon after birth, whereas high levels of *Klf7* activity in the adult brain are mostly confined to the cerebellum, hippocampus, and OBs (32). Histological analyses of neonatal (P1) *Klf7*$^{-/-}$ brains revealed severe perturbations of the tracts that constitute the major forebrain connections (Fig. 5a). Specifically, we found that the fibers of the corpus callosum do not cross the midline, the anterior commissure is missing or severely disrupted, and the fimbria is reduced in size (Fig. 5b and data not shown). TAG-1 immunofluorescence documented the failure of cortical efferent projections to enter the internal capsule (Fig. 5c) (20). The comparable intensity of the TAG-1 signal in the mutant and wild-type brains suggested that the defect is not probably accounted for by a substantial reduction in the number of TAG-1-positive cortical neurons (Fig. 5c). L1 is an adhesion molecule widely expressed in several neuronal populations, including those forming cortical afferent fibers (20). L1 immunofluorescence showed that cortical afferent fibers in *Klf7*-null brains are hyperfasciculated and that medial tracts are misrouted just before entering the cortical fiber layer (Fig. 5d). GAP43 immunohistochemistry documented the same deficiencies in E16.5 mutant brains, thus suggesting that the cortical phenotype is probably not caused by excessive neuronal retraction and pruning after improper targeting (data not shown).

The cortical deficits described above could result from defective migration of progenitor cell migration, a process which is ultimately responsible for the formation of the multiple layers of the cerebral cortex (Fig. 5a) (1). However, standard histology revealed a seemingly normal cortical layering in the mutant P1 brain (Fig. 6a). This finding was extended at the molecular level by performing in situ hybridizations with probes specific for different layers of the cerebral cortex. They included *Foxp2*, which recognizes the neurons of the deeper layer 6; *ROR*β, which is specific for cells in layers IV and V; *Foxp1*, which is a marker for cells in layers III to V; and *reelin*, which is expressed by the Cajal-Retzius neurons in the outermost layer of the cortex (Fig. 6b) (3, 18, 43). The results of these in situ hybridizations failed to detect significant differences between mutant and wild-type cortices (Fig. 6b). However, a histomorphometric analysis estimated that the *Klf7*$^{-/-}$

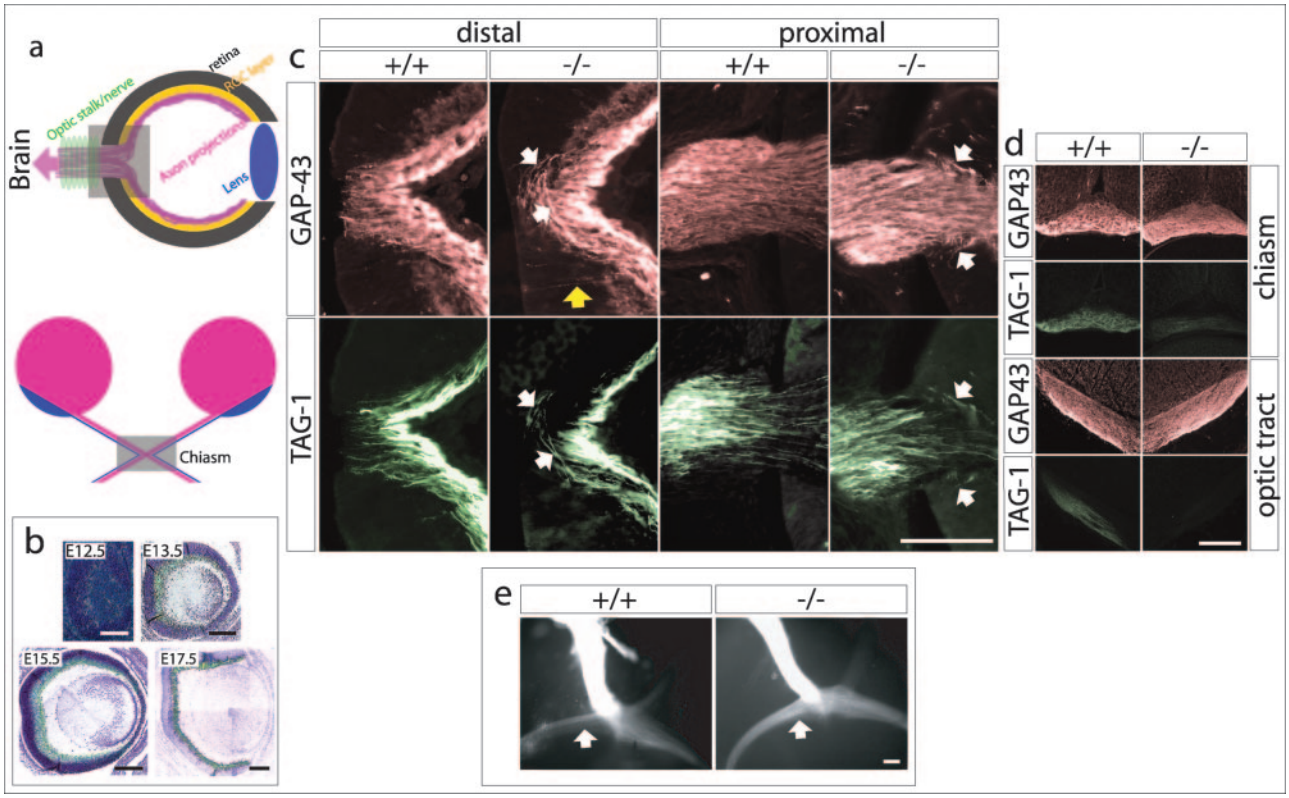

FIG. 4. Axon guidance defects in the *Klf7*$^{-/-}$ visual system at P1. (a) Top: schematic representation of an eye cross section showing the RGC layer (yellow) and their projections (purple) to the inner retinal surface, the optic disk, and optic stalk. The field of view shown in panel c is shaded in grey. Bottom: schematic representation of contralateral and ipsilateral RGC projections from the eyes through the chiasm. The field of view shown in panel e is shaded in grey. (b) Profile of *Klf7* expression in the developing eye. Shown are in situ hybridizations of coronal sections through the eye to a *Klf7* probe. The signal was pseudocolored in green and merged with the respective histological image; only the E12.5 image was left in the original dark-field form. Bars, 300 μm. (c) Axon guidance errors in the *Klf7*$^{-/-}$ optic disk. The fields of view are orientated as indicated in panel a, top; axons were visualized using the indicated antibodies. "Distal" sections were cut along the periphery of the optic disk; "proximal" sections were cut along the center. White arrows highlight axons turning away from the optic disk and failing to grow into the optic stalk. The yellow arrow indicates the axon exiting the retinal nerve layer prematurely and growing towards the periphery ($n = 6$ per genotype). (d) Coronal sections through the optic chiasm and tract showing that TAG-1-positive fibers fail to grow beyond the mutant chiasm ($n = 8$ per genotype). (e) The ipsilateral component appears to be enlarged in the postnatal day 1 *Klf7*$^{-/-}$ optic chiasm (arrows), as visualized with anterograde DiI labeling in whole-mount preparations ($n = 4$ per genotype). Bars (except panel b), 100 μm.

cortex is ~30% thinner than the wild-type counterpart (Fig. 6c). Although the phenotype could be caused in part by thinner white matter tracts, additional analyses revealed that there are ~15% fewer cells in the mutant than in the wild-type cortex (Fig. 6c). Likewise, immunofluorescence using a generic neuronal marker, TuJ, showed a slightly less intense staining in the mutant than in wild-type cortex (Fig. 6d). However, neither the TUNEL assay nor phospho-histone 3 immunohistochemistry correlated the morphological defect with statistically significant changes in cell death or proliferation (data not shown). Lacking additional evidence, we concluded that the dramatic loss of axon growth and consequently of target innervation in the *Klf7* null brain may have compromised neuronal survival below the threshold of experimental detection.

In addition to defects in axon projections, we also identified abnormalities in dendritic organization in *Klf7*-null brains, notably in the adult hippocampus (Fig. 7) (27). Golgi-Cox staining in fact showed that the complexity of both apical and basal dendritic trees of CA1 pyramidal cells is reduced (Fig. 7c and d) (27). There were also abnormal arbors of cortical neurons, granule cells of the dentate gyrus, and the major fiber tracts (data not shown). In contrast to the cerebral cortex and hippocampus, no defects were noted in another location of high *Klf7* expression in the brain, the cerebellum (data not shown). Together, these observations therefore documented the role of KLF7 in guiding neurite outgrowth at selected anatomical locations of the CNS.

KLF7 regulates neuronal morphogenesis in part through Cip/Kip stimulation. We have recently shown that KLF7 stimulates *p21*$^{cip/waf}$ transcription by directly binding to the proximal promoter sequence (56). Others had previously reported accumulation of p21$^{cip/waf}$ in the differentiating neurons of the postnatal OE (34). Based on these lines of evidence, we compared the expression levels of *p21*$^{cip/waf}$ in mutant and wild-type OE from embryos and newborn mice. In situ hybridizations and immunoblot assays estimated that *p21*$^{cip/waf}$ gene activity in the mutant OE is significantly less than normal (Fig. 8a and b). Furthermore, immunoblots of protein extracts from wild-type and mutant OE of P1 mice revealed a similar decrease in p27^{kip1} protein levels and no detectable changes in

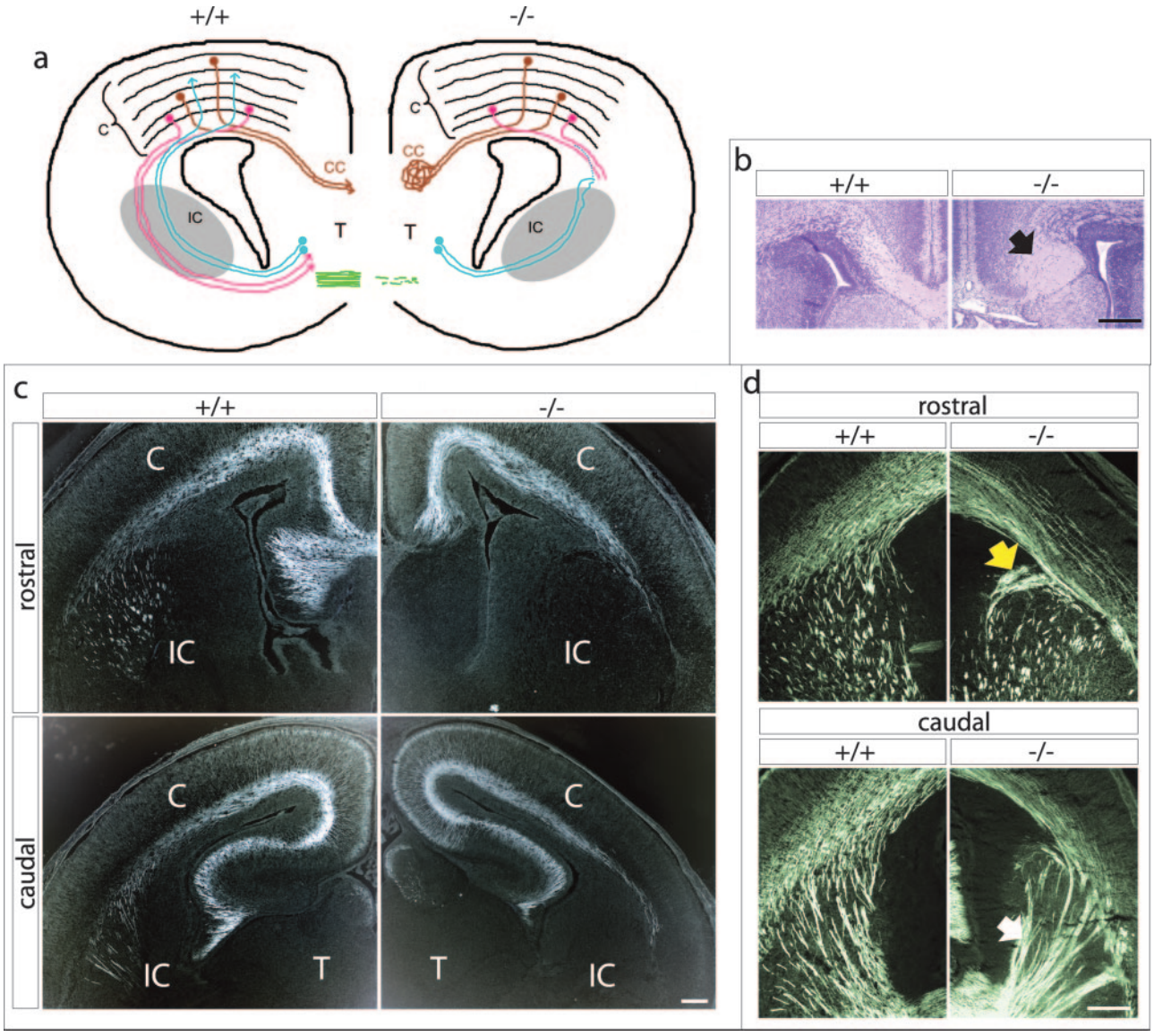

FIG. 5. Defective fiber tracts in *Klf7*$^{-/-}$ brains at P1. (a) Scheme of relevant fiber tracts and cortical layering in the wild-type (left) and mutant (right) brains shown in the same coronal plane as the sections in panels b to d. Tracts are color coded as follows: blue, cortical afferent; red, cortical efferent; brown, corpus callosum; green, anterior commissure. Color-coded filled circles represent the originating neurons, and the arrowheads represent the corresponding axon ends. The shaded grey area represents the internal capsule, through which cortical efferent axons grow normally in the wild-type but not in the mutant mice. Abbreviations: C, cortical layers; CC, corpus callosum; IC, internal capsule; T, thalamus. (b) Sections stained by hematoxylin and eosin to reveal the corpus callosum (arrow indicates abnormal corpus callosum in the mutant); $n = 10$ per genotype. (c) Sections stained by anti-TAG-1 antibodies to visualize cortical efferent projections at two levels along the rostral-caudal axis ($n = 6$ per genotype). (d) Sections stained by anti-L1 antibodies to visualize cortical afferent projections at two levels along the rostral-caudal axis. The yellow arrow indicates fiber misprojection, whereas the white arrow highlights axon hyperfasciculation ($n = 6$ per genotype). Bars, 200 μm.

p57^{kip2} (Fig. 8b). This last result raised the possibility that *p27^{kip1}* may be another gene targeted by KLF7. To test this hypothesis, a KLF7 expression plasmid was cotransfected with a luciferase reporter gene construct harboring the proximal promoter of the *p27^{kip1}* gene (40). These in vitro assays showed that KLF7 can stimulate transcription from the *p27^{kip1}* promoter nearly 10-fold (Fig. 8c). Additionally, we performed ChIP experiments in 293T cells transfected with the KLF7 expression plasmid and found that the transcription factor binds to the proximal promoter sequence of the endogenous *p27^{kip1}* gene (Fig. 8d). Together with the in vivo findings, transfection and ChIP experiments established that two members of the Cip/Kip family of cdk inhibitors are directly regulated by KLF7.

Recent studies have demonstrated that the Cip/Kip proteins have additional functions outside the nucleus that are unrelated to the cell cycle, such as regulating neurite remodeling (14). We therefore examined the intracellular distribution in wild-type OSN cultures of the two Cip/Kip proteins whose expression is affected by loss of *Klf7*. Unlike immature neurons or nonneuronal cells, differentiating OSNs displayed significant amounts of p21$^{cip/waf}$ and p27^{kip1} in the cytosolic com-

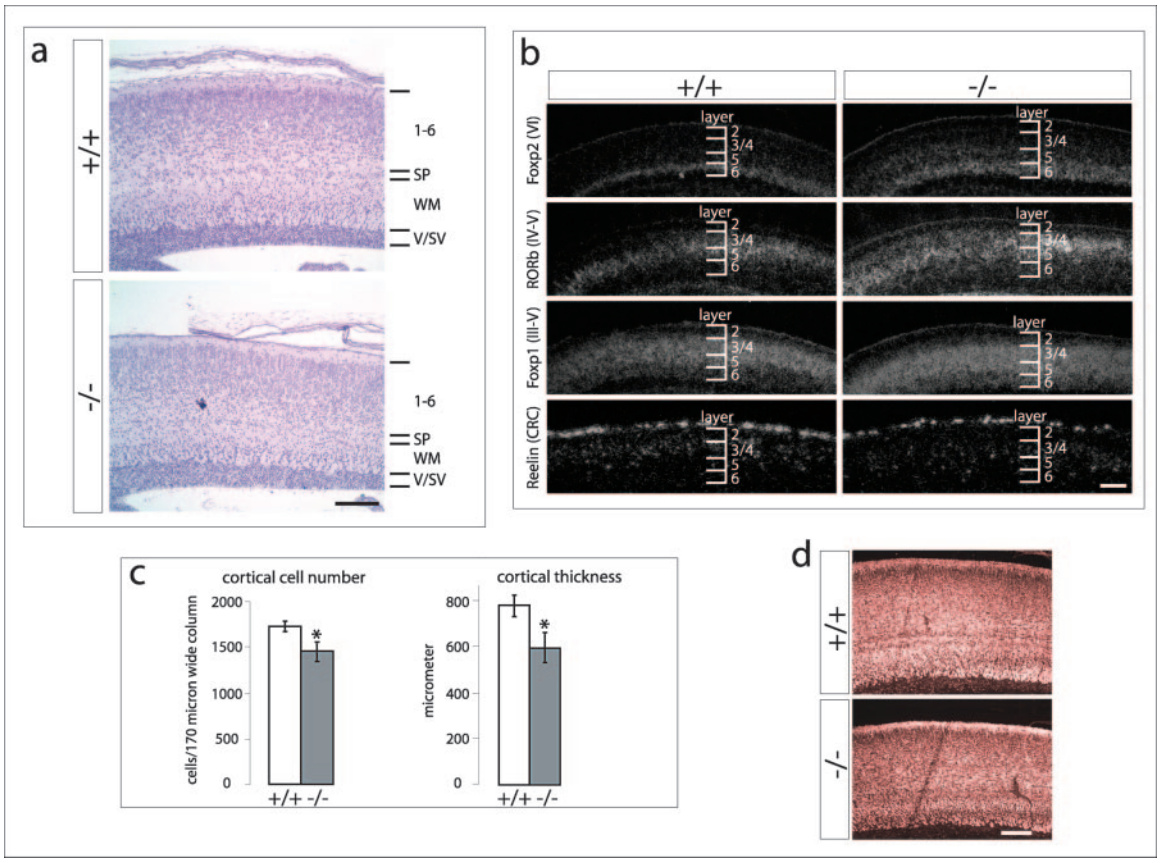

FIG. 6. Normal layering of the *Klf7*$^{-/-}$ cerebral cortex at P1. All sections are sagittal; dorsal is up, and rostral is left. (a) Hematoxylin and eosin staining showing normal organization of the cortical layers in *Klf7*$^{-/-}$ brains (also Fig. 5a). Abbreviations: SP, subplate; SV, subventricular zone; V, ventricular zone; WM, white matter; 1-6, cortical layers ($n = 4$ per genotype). (b) In situ hybridizations to the indicated probes show normal expression of layer-specific molecular markers in the *Klf7*$^{-/-}$ cortex. CRC, Cajal-Retzius cells; numbers indicate cortical layers ($n = 3$ per genotype). (c) Histomorphometric comparison of the wild-type and mutant cortex. Bar graphs reflect the means ± standard deviations. *, significance: $P < 0.02$ (Student's unpaired t test); $n = 5$ per genotype and analysis. (d) Neurons visualized by anti-TuJ immunofluorescence; $n = 5$ per genotype. Bars, 200 μm.

partment, including axonal and dendritic extensions (Fig. 8e). The quantity, but not the intracellular localization, of p21$^{cip/waf}$ was significantly reduced in *Klf7*$^{-/-}$ OSNs (Fig. 8f). We interpreted these results to suggest that KLF7 may act on neuronal morphogenesis in part by reducing the relative levels of molecules that may promote neurite outgrowth.

DISCUSSION

The results of the present study imply a function for KLF7 in neuronal morphogenesis and thus in the establishment of connectivity at several distinct anatomical sites in the CNS and peripheral nervous system. A role for the transcription factor in neurogenesis was previously suggested by gene expression studies that documented high *Klf7* activity in selected neuronal subtypes of the developing embryo and adult organism (32, 35). Here we have shown that absence of KLF7 affects neurite outgrowth. This observation is consistent with the prevalent expression of the transcription factor in postmitotic and not in proliferating neurons (32). The most evident anatomical consequence of loss of KLF7 activity was seen in the olfactory system, in the form of severely hypoplastic bulbs lacking peripheral innervation. In vivo evidence indicates that part of KLF7 action on OSN differentiation is to establish optimal levels of p21$^{cip/waf}$ and p27^{kip1} synthesis. We speculate from correlative data in the literature and our own in vitro analyses that KLF7 stimulation of *p21*$^{cip/waf}$ and *p27*^{kip1} transcription may ultimately impact on cytoskeletal dynamics that promote neurite outgrowth. Irrespective of the underlying mechanism, our genetic evidence adds the nervous system to the list of organs and tissues whose development is regulated by members of the KLF family.

The olfactory nerve defect in *Klf7*$^{-/-}$ mice is apparent as early as the stage in which OSNs first project towards the forebrain in an otherwise anatomically normal olfactory cavity (6). This last observation together with *Klf7*-restricted expression in the OE excludes the possibility that loss of signals emanating from the surrounding mesenchyme may contribute to the mutant OE phenotype. We have also presented evidence indicating that the mutation has no significant negative effects on OE cell survival or proliferation and consequently on the thickness and cell density of the mutant tissue. Although absence of afferent innervation has been also observed in the olfactory system of *Pax6*, *Gli3*, *Emx2*, and *Dlx5* mutant mice,

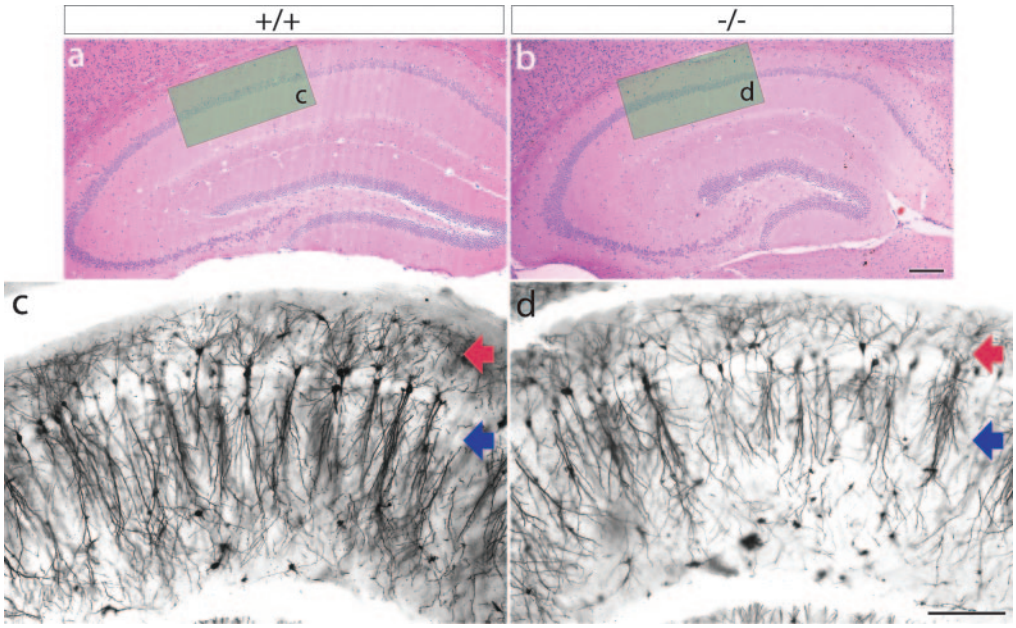

FIG. 7. Impaired dendritic arborization of pyramidal neurons in the adult *Klf7*$^{-/-}$ hippocampus. (a and b) Coronal sections through adult hippocampi were stained by hematoxylin and eosin; shaded areas correspond to the fields displayed in panels c and d. (c and d) Abnormal dendritic arborization of CA1 pyramidal neurons in the mutant hippocampus revealed by Golgi-Cox staining. Red and blue arrows indicate the apical and basal side of CA1 pyramids, respectively (n = 3 per genotype). Bars, 200 μm.

the phenotype is significantly more severe in these animals than in *Klf7*-null mice (25, 36, 59, 63). This and preliminary evidence showing normal expression of the aforementioned genes in the *Klf7*-null OE and vice versa suggest that KLF7 operates on a separate pathway from transcription factors Dlx5 and Gli3/Emx2 during olfactory neurogenesis. OB hypoplasia in *Klf7*$^{-/-}$ mice, on the other hand, is in line with the current model of bulb development, which postulates that onset of neurogenesis and bulb evagination are innervation-independent processes (25, 36, 59, 63). Work in progress is examining the olfactory system of those rare *Klf7*-null mice that survive into adulthood in order to assess whether a potential contribution of peripheral innervation to bulb maturation and morphogenesis may exist.

By analogy to the olfactory system, restricted *Klf7* expression in the forming RGCs and the overall normal anatomy of the mutant eye argue for a cell-autonomous defect causing impaired axonal growth in the visual system. A number of transcription factors have been identified that modulate the formation of the optic nerve and optic tract, but only some appear to affect RGC morphogenesis in a cell-autonomous manner (17, 22). For example, *Brn-3.2* displays the same expression pattern in the eye as *Klf7* does, and mice lacking this transcription factor are characterized by aberrant RGC projections towards the optic disk (17). Erkman et al. (17) have shown that *Brn-3.2* controls axon pathfinding in part by regulating the expression of the actin-binding protein mabLIM. Whether *Brn-3.2* and/or *mabLIM* expression is affected in the *Klf7*$^{-/-}$ retina remains to be determined. The absence of expression of TAG-1 in the optic tract in the *Klf7*-null embryos is reminiscent of TAG-1 in the spinal cord, where the TAG-1 gene is downregulated in commissural axons after decussation (15). It is possible that guidance errors or disorganization of axons at the chiasm, as demonstrated with the increase in ipsilateral projections, results in this decreased TAG-1 expression. Although preferential expression of TAG-1 in the ventral optic nerve is a novel finding, two TAG-1-related cell adhesion molecules, PSA-NCAM and L1, have been recently reported to be more strongly expressed in the dorsal than the ventral portion of the optic tract (7).

Similar to the olfactory and optic systems, brain abnormalities in *Klf7*-null mice appear to involve distinct pathways compared to similar phenotypes of mice lacking other transcription factors, such as Coup-tf1 or Tbr-1 (23, 64). *Coup-tf1*-null mice display a lack of thalamocortical input to the cortex and aberrant differentiation and apoptosis of subplate neurons (64). Since subplate neurons are crucial for proper thalamocortical projections, the thalamocortical defect of *Coup-tf1*-null mice is likely to represent a secondary effect of the mutation (64). By contrast, the fact that the subplate in *Klf7*$^{-/-}$ brains is unaffected gives credence to the notion that the abnormal thalamocortical trajectory in these mutant mice is a primary rather than a secondary defect. Thalamocortical and subplate abnormalities, as well as defects in the corpus callosum and corticothalamic projections, characterize *Tbr1*$^{-/-}$ mice (23). However, these animals also display cortical cell migration defects leading to cortical inversion, which may conceivably contribute to subplate and projection abnormalities (23). We have tested *Klf7*$^{-/-}$ mice for potential cortical migration defects and found none. On the other hand, we were unable to explain the precise origin of the cellular deficit in the *Klf7*-null cortex. Finally, the finding of significant neurite deficits in the hippocampus raises the possibility that maintenance of KLF7 activity throughout adulthood may be crucial for neuronal wiring and implicitly for learning processes localized to this area of the brain (27).

Loss of KLF7 activity is predicted to affect the expression of

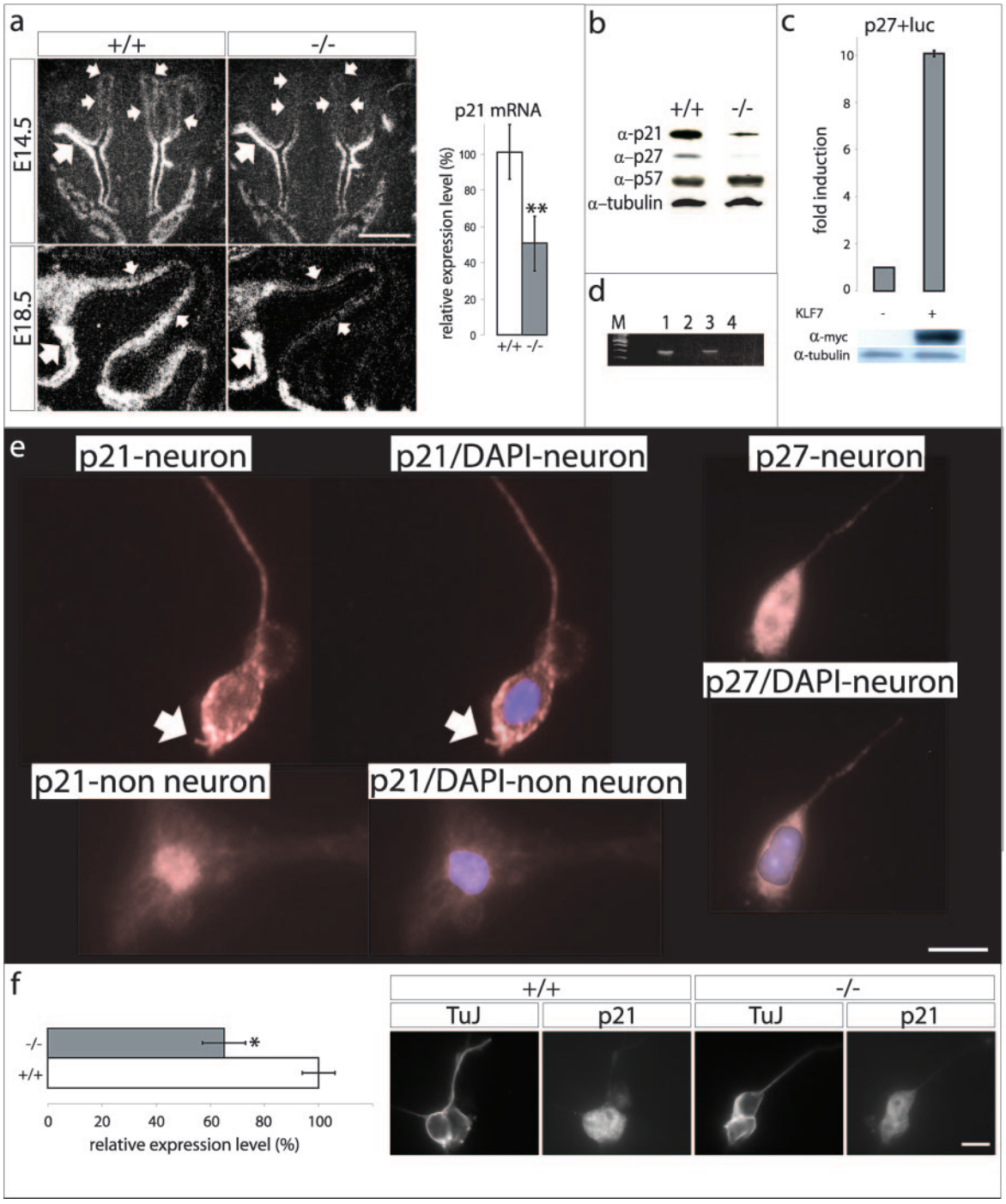

FIG. 8. Cip/Kip expression in the *Klf7*$^{-/-}$ olfactory system. (a) In situ hybridizations of coronal and sagittal OE sections from E.14.5 and E18.5, respectively, wild-type and mutant mice to a *p21*$^{waf/cip}$ riboprobe. Unlike in the OE (small arrows), *p21*$^{waf/cip}$ expression in the adjacent airway epithelium is unaffected (large arrows) ($n = 3$ per genotype for E14.5). Of note, *p21*$^{waf/cip}$ expression is reduced in the mutant OE as early as E14.5. On the right, bar graphs indicate the mean mRNA levels ± standard deviations calculated for eight animals per genotype (E18.5) using Metamorph software. The *Klf7*$^{+/+}$ mean was set as 100%. **, significance: $P < 0.005$ (Student's unpaired *t* test). (b) Western analysis of p21$^{waf/cip}$, p27^{kip1}, p57^{kip2}, and tubulin levels in the postnatal OE from wild-type and mutant animals. (c) Cotransfection of NIH 3T3 fibroblasts with 200 ng of KLF7 expression plasmid and with 100 ng of the *p27*^{kip1} promoter/luciferase construct. The bar graph indicates the mean fold of induction ± standard deviation. Shown below are immunoblots showing the levels of the cMyc-KLF7 fusion protein (α-Myc) compared to endogenous tubulin (α-tubulin) in the indicated cells. (d) KLF7 binds in vivo to the *p27*^{kip1} promoter. Shown are results of ChIP analysis of mock-transfected cells before (lane 1) and after (lane 2) immunoprecipitation with anti-Myc antibody and from Myc-tagged KLF7-transfected cells following immunoprecipitation with (lane 3) and without (lane 4) anti-Myc antibody. The PCR *p27*^{kip1} product is 250 bp; lane M, DNA markers. (e) Representative immunofluorescence detection of cytoplasmic p21$^{waf/cip}$ and p27^{kip1} protein in cultured OSNs from wild-type mice is shown; 40 cells were analyzed for each staining. Nuclei were stained with DAPI. Arrows indicate small dendrite-like outgrowth. (f) Expression of p21$^{waf/cip}$ protein is reduced in cultured *Klf7*$^{-/-}$ OSNs. Bar graphs reflect the means ± standard errors of the means. *, significance: $P < 0.05$ (Student's unpaired *t* test); $n = 20$ cells per genotype. The *Klf7*$^{+/+}$ mean was set as 100%. Representative micrographs of p21$^{waf/cip}$ and corresponding TuJ expression are shown. Bars, 500 μm (a) and 10 μm (e and f).

multiple genes and intracellular pathways either directly or indirectly. Significant downregulation (but not loss) of *p21$^{cip/waf}$* expression in the mutant OE is an important finding of our study, which demonstrates a functional relationship between this multifunctional protein and OSN differentiation. The finding is in line with the well-established contribution of p21$^{cip/waf}$ to terminal differentiation of several cell lineages through negative or positive mechanisms and in connection with or independent of cell cycle regulation (16). Legrier et al. (34) have interpreted gene expression data to indicate that individual cdk inhibitors fulfill distinct roles in OE neurogenesis, including maintenance of a quiescent phenotype (p21$^{cip/waf}$) and control of cell cycle withdrawal (p27^{kip1}). These last data, however, seem to contrast the apparent lack of OSN defects in p21$^{waf/cip}$- and p27^{kip1}-deficient mice, a problem which probably reflects the different focuses of these earlier analyses (13, 19).

We can only speculate from correlative evidence in the literature and our study about the mechanistic relationship between downregulation of p21$^{cip/waf}$ and p27^{kip1} and impaired neurite outgrowth in *Klf7*-null OSNs. A large body of work has established the multiple functions of the actin cytoskeleton in axon initiation, growth, guidance, and branching, as well as the role of the Rho family of small GTPases in regulating neuronal morphogenesis (21, 37). Evidence has been presented that signaling of many axon guidance receptors converges onto Rho, Rac, and/or Cdc42, which in turn activate downstream targets, like Rho-kinase (ROCK), which remodel the cytoskeleton (37). Recent studies of a variety of cell systems, including differentiating neurons, have shown that Cip/Kip proteins regulate actin dynamics through inhibition of the Rho-ROCK-LIMK pathway (4, 14, 57, 62). One of them, in particular, has documented the ability of cytoplasmic p21$^{cip/waf}$ to promote axonal regeneration and functional recovery in a rat model of spinal injury (58). In the present study, we have shown that p21$^{cip/waf}$ displays a cytoplasmic localization in differentiating OSNs; additionally, we have made an indirect connection between loss of KLF7 activity and impaired neurite growth by associating p21$^{cip/waf}$ downregulation in the mutant OE and cultured OSNs. Accordingly we propose that KLF7 may promote neuronal morphogenesis in part by increasing the overall (and cytosolic) levels of p21$^{cip/waf}$ and p27^{kip1}. A similar mechanism may also operate in the accessory olfactory system of the *Klf7*-null mice in which there are fewer and poorly projecting mature sensory neurons and substantial *p21$^{cip/waf}$* downregulation (our unpublished data). Furthermore, this functional relationship may extend to other regions of the neonatal and adult brain where *Klf7* and Cip/Kip genes are coexpressed, such as the OBs, cerebral cortex, and hippocampus (32, 47, 52, 60). Irrespective of the underlying mechanism in OE neurogenesis and its relevance to other regions of the nervous system, our findings are the first to demonstrate a role for p21$^{cip/waf}$ and p27^{kip1} in the differentiation of olfactory neurons.

As we have previously shown for *p21$^{cip/waf}$* (56), cotransfection and ChIP experiments have established that the *p27^{kip1}* gene is a transcriptional target of KLF7. Several KLFs have been shown to stimulate transcription from the *p21$^{cip/waf}$* promoter, thus raising the possibility of functional redundancy in cell types where they are coexpressed (5, 10, 26). KLF6 and KLF7 are a case in point. They constitute a structurally distinct group within the KLF family, which shares a common progenitor in invertebrates (11); they have identical transactivation domains, which stimulate the *p21$^{cip/waf}$* promoter in cotransfection assays (32, 44, 56); and the corresponding genes are coexpressed in a few locations of the nervous system, including cortical neurons, DRG, and neural tube (32, 33). Although we noted *Klf6* upregulation in *Klf7*-null neurons, early embryonic lethality of *Klf6*-null mice has hampered the analysis of the genetic interaction between these two loci (our unpublished data). Finally, it is interesting that KLF7 function in neurogenesis is consistent with a recent report of a chromosomal deletion that includes the *KLF7* gene in a human patient with neurodevelopmental abnormalities (49). That *Klf7* loss impairs neurite outgrowth without disturbing overall tissue architecture and morphology of the nervous system makes the *Klf7*$^{-/-}$ mice an informative model in which to dissect the histological complexity of mammalian axogenesis.

ACKNOWLEDGMENTS

We thank F. Margolis, P. Mombaerts, G. Sonenshein, T. Curran, and B. Vogelstein for providing critical reagents; T. Sakurai for invaluable comments on the manuscript; S. Lee-Arteaga and C. Else for excellent technical assistance; and K. Johnson for preparing the manuscript.

This work was supported by NIH grants NS33199 (L. F. Parada) and AR38648, the New York State Spinal Cord Injury Research Program, the St. Giles Foundation, and the James D. Farley family.

REFERENCES

1. **Allendoerfer, K. L., and C. J. Shatz.** 1994. The subplate, a transient neocortical structure: its role in the development of connections between thalamus and cortex. Annu. Rev. Neurosci. **17:**185–218.
2. **Baker, H., D. M. Cummings, S. D. Munger, J. W. Margolis, L. Franzen, R. R. Reed, and F. L. Margolis.** 1999. Targeted deletion of a cyclic nucleotide-gated channel subunit (OCNC1): biochemical and morphological consequences in adult mice. J. Neurosci. **19:**9313–9321.
3. **Bar, I., and A. M. Goffinet.** 2000. Evolution of cortical lamination: the reelin/Dab1 pathway. Novartis Found. Symp. **228:**114–128.
4. **Besson, A., M. Gurian-West, A. Schmidt, A. Hall, and J. M. Roberts.** 2004. p27^{Kip1} modulates cell migration through the regulation of RhoA activation. Genes Dev. **18:**862–876.
5. **Bieker, J. J.** 2001. Kruppel-like factors: three fingers in many pies. J. Biol. Chem. **276:**34355–34358.
6. **Calof, A. L., J. S. Mumm, P. C. Rim, and J. Shou.** 1998. The neuronal stem cell of the olfactory epithelium. J. Neurobiol. **36:**190–205.
7. **Chung, K. Y., K. M. Leung, C. C. Lin, K. C. Tam, Y. L. Hao, J. S. Taylor, and S. O. Chan.** 2004. Regionally specific expression of L1 and sialylated NCAM in the retinofugal pathway of mouse embryos. J. Comp. Neurol. **471:**482–498.
8. **Coghill, E., S. Eccleston, V. Fox, L. Cerruti, C. Brown, J. Cunningham, S. Jane, and A. Perkins.** 2001. Erythroid Kruppel-like factor (EKLF) coordinates erythroid cell proliferation and hemoglobinization in cell lines derived from EKLF null mice. Blood **97:**1861–1868.
9. **Danciger, E., C. Mettling, M. Vidal, R. Morris, and F. Margolis.** 1989. Olfactory marker protein gene: its structure and olfactory neuron-specific expression in transgenic mice. Proc. Natl. Acad. Sci. USA **86:**8565–8569.
10. **Dang, D. T., J. Pevsner, and V. W. Yang.** 2000. The biology of the mammalian Kruppel-like family of transcription factors. Int. J. Biochem. Cell Biol. **32:**1103–1121.
11. **De Graeve, F., S. Smaldone, F. Laub, M. Mlodzik, M. Bhat, and F. Ramirez.** 2003. Identification of the Drosophila progenitor of mammalian Kruppel-like factors 6 and 7 and a determinant of fly development. Gene **314:**55–62.
12. **Deiner, M. S., T. E. Kennedy, A. Fazeli, T. Serafini, M. Tessier-Lavigne, and D. W. Sretavan.** 1997. Netrin-1 and DCC mediate axon guidance locally at the optic disc: loss of function leads to optic nerve hypoplasia. Neuron **19:**575–589.
13. **Deng, C., P. Zhang, J. W. Harper, S. J. Elledge, and P. Leder.** 1995. Mice lacking p21$^{CIP1/WAF1}$ undergo normal development, but are defective in G1 checkpoint control. Cell **82:**675–684.
14. **Denicourt, C., and S. F. Dowdy.** 2004. Cip/Kip proteins: more than just CDKs inhibitors. Genes Dev. **18:**851–855.
15. **Dodd, J., S. B. Morton, D. Karagogeos, M. Yamamoto, and T. M. Jessell.**

1988. Spatial regulation of axonal glycoprotein expression on subsets of embryonic spinal neurons. Neuron **1:**105–116.
16. **Dotto, G. P.** 2000. p21(WAF1/Cip1): more than a break to the cell cycle? Biochim. Biophys. Acta **1471:**M43–M56.
17. **Erkman, L., P. A. Yates, T. McLaughlin, R. J. McEvilly, T. Whisenhunt, S. M. O'Connell, A. I. Krones, M. A. Kirby, D. H. Rapaport, J. R. Bermingham, D. D. O'Leary, and M. G. Rosenfeld.** 2000. A POU domain transcription factor-dependent program regulates axon pathfinding in the vertebrate visual system. Neuron **28:**779–792.
18. **Ferland, R. J., T. J. Cherry, P. O. Preware, E. E. Morrisey, and C. A. Walsh.** 2003. Characterization of Foxp2 and Foxp1 mRNA and protein in the developing and mature brain. J. Comp. Neurol. **460:**266–279.
19. **Fero, M. L., M. Rivkin, M. Tasch, P. Porter, C. E. Carow, E. Firpo, K. Polyak, L. H. Tsai, V. Broudy, R. M. Perlmutter, K. Kaushansky, and J. M. Roberts.** 1996. A syndrome of multiorgan hyperplasia with features of gigantism, tumorigenesis, and female sterility in p27(Kip1)-deficient mice. Cell **85:**733–744.
20. **Fujimori, K. E., K. Takeuchi, T. Yazaki, K. Uyemura, Y. Nojyo, and N. Tamamki.** 2000. Expression of L1 and TAG-1 in the corticospinal, callosal, and hippocampal commissural neurons in the developing rat telencephalon as revealed by retrograde and in situ hybridization double labeling. J. Comp. Neurol. **417:**275–288.
21. **Guan, K. L., and Y. Rao.** 2003. Signalling mechanisms mediating neuronal responses to guidance cues. Nat. Rev. Neurosci. **4:**941–956.
22. **Herrera, E., L. Brown, J. Aruga, R. A. Rachel, G. Dolen, K. Mikoshiba, S. Brown, and C. A. Mason.** 2003. Zic2 patterns binocular vision by specifying the uncrossed retinal projection. Cell **114:**545–557.
23. **Hevner, R. F., L. Shi, N. Justice, Y. Hsueh, M. Sheng, S. Smiga, A. Bulfone, A. M. Goffinet, A. T. Campagnoni, and J. L. Rubenstein.** 2001. Tbr1 regulates differentiation of the preplate and layer 6. Neuron **29:**353–366.
24. **Huber, T. L., A. C. Perkins, A. E. Deconinck, F. Y. Chan, P. E. Mead, and L. I. Zon.** 2001. neptune, a Kruppel-like transcription factor that participates in primitive erythropoiesis in Xenopus. Curr. Biol. **11:**1456–1461.
25. **Jimenez, D., C. Garcia, F. de Castro, A. Chedotal, C. Sotelo, J. A. de Carlos, F. Valverde, and L. Lopez-Mascaraque.** 2000. Evidence for intrinsic development of olfactory structures in Pax-6 mutant mice. J. Comp. Neurol. **428:**511–526.
26. **Kaczynski, J., T. Cook, and R. Urrutia.** 2003. Sp1- and Kruppel-like transcription factors. Genome Biol. **4:**206.
27. **Kandel, E. R., J. S. Schwartz, and T. M. Jessell.** 2000. Principles of neuroscience, 4th ed. McGraw-Hill, New York, N.Y.
28. **Katz, J. P., N. Perreault, B. G. Goldstein, C. S. Lee, P. A. Labosky, V. W. Yang, and K. H. Kaestner.** 2002. The zinc-finger transcription factor Klf4 is required for terminal differentiation of goblet cells in the colon. Development **129:**2619–2628.
29. **Kawahara, A., and I. B. Dawid.** 2001. Critical role of biklf in erythroid cell differentiation in zebrafish. Curr. Biol. **11:**1353–1357.
30. **Kuo, C. T., M. L. Veselits, K. P. Barton, M. M. Lu, C. Clendenin, and J. M. Leiden.** 1997. The LKLF transcription factor is required for normal tunica media formation and blood vessel stabilization during murine embryogenesis. Genes Dev. **11:**2996–3006.
31. **Kuo, C. T., M. L. Veselits, and J. M. Leiden.** 1997. LKLF: a transcriptional regulator of single-positive T cell quiescence and survival. Science **277:**1986–1990.
32. **Laub, F., R. Aldabe, V. Friedrich, Jr., S. Ohnishi, T. Yoshida, and F. Ramirez.** 2001. Developmental expression of mouse Kruppel-like transcription factor KLF7 suggests a potential role in neurogenesis. Dev. Biol. **233:**305–318.
33. **Laub, F., R. Aldabe, F. Ramirez, and S. Friedman.** 2001. Embryonic expression of Kruppel-like factor 6 in neural and non-neural tissues. Mech. Dev. **106:**167–170.
34. **Legrier, M. E., A. Ducray, A. Propper, M. Chao, and A. Kastner.** 2001. Cell cycle regulation during mouse olfactory neurogenesis. Cell Growth Differ. **12:**591–601.
35. **Lei, L., L. Ma, S. Nef, T. Thai, and L. F. Parada.** 2001. mKlf7, a potential transcriptional regulator of TrkA nerve growth factor receptor expression in sensory and sympathetic neurons. Development **128:**1147–1158.
36. **Long, J. E., S. Garel, M. J. Depew, S. Tobet, and J. L. Rubenstein.** 2003. DLX5 regulates development of peripheral and central components of the olfactory system. J. Neurosci. **23:**568–578.
37. **Luo, L.** 2002. Actin cytoskeleton regulation in neuronal morphogenesis and structural plasticity. Annu. Rev. Cell Dev. Biol. **18:**601–635.
38. **Lustig, M., L. Erskine, C. A. Mason, M. Grumet, and T. Sakurai.** 2001. Nr-CAM expression in the developing mouse nervous system: ventral midline structures, specific fiber tracts, and neuropilar regions. J. Comp. Neurol. **434:**13–28.
39. **Matsumoto, N., F. Laub, R. Aldabe, W. Zhang, F. Ramirez, T. Yoshida, and M. Terada.** 1998. Cloning the cDNA for a new human zinc finger protein defines a group of closely related Kruppel-like transcription factors. J. Biol. Chem. **273:**28229–28237.
40. **Minami, S., N. Ohtani-Fujita, E. Igata, T. Tamaki, and T. Sakai.** 1997. Molecular cloning and characterization of the human $p27^{Kip1}$ gene promoter. FEBS Lett. **411:**1–6.
41. **Mombaerts, P., F. Wang, C. Dulac, S. K. Chao, A. Nemes, M. Mendelsohn, J. Edmondson, and R. Axel.** 1996. Visualizing an olfactory sensory map. Cell **87:**675–686.
42. **Nagy, A., M. Gertsenstein, K. Vintersten, and R. Behringer.** 2003. Manipulating the mouse embryo: a laboratory manual, 3rd ed. Cold Spring Harbor Laboratory Press, Cold Spring Harbor, N.Y.
43. **Nakagawa, Y., and D. D. O'Leary.** 2003. Dynamic patterned expression of orphan nuclear receptor genes RORα and RORβ in developing mouse forebrain. Dev. Neurosci. **25:**234–244.
44. **Narla, G., K. E. Heath, H. L. Reeves, D. Li, L. E. Giono, A. C. Kimmelman, M. J. Glucksman, J. Narla, F. J. Eng, A. M. Chan, A. C. Ferrari, J. A. Martignetti, and S. L. Friedman.** 2001. KLF6, a candidate tumor suppressor gene mutated in prostate cancer. Science **294:**2563–2566.
45. **Nuez, B., D. Michalovich, A. Bygrave, R. Ploemacher, and F. Grosveld.** 1995. Defective haematopoiesis in fetal liver resulting from inactivation of the EKLF gene. Nature **375:**316–318.
46. **Oates, A. C., S. J. Pratt, B. Vail, Y. Yan, R. K. Ho, S. L. Johnson, J. H. Postlethwait, and L. I. Zon.** 2001. The zebrafish klf gene family. Blood **98:**1792–1801.
47. **Parker, S. B., G. Eichele, P. Zhang, A. Rawls, A. T. Sands, A. Bradley, E. N. Olson, J. W. Harper, and S. J. Elledge.** 1995. p53-independent expression of $p21^{Cip1}$ in muscle and other terminally differentiating cells. Science **267:**1024–1027.
48. **Perkins, A. C., A. H. Sharpe, and S. H. Orkin.** 1995. Lethal beta-thalassaemia in mice lacking the erythroid CACCC-transcription factor EKLF. Nature **375:**318–322.
49. **Pescucci, C., I. Meloni, M. Bruttini, F. Ariani, I. Longo, F. Mari, R. Canitano, G. Hayek, M. Zappella, and A. Renieri.** 2003. Chromosome 2 deletion encompassing the MAP2 gene in a patient with autism and Rett-like features. Clin. Genet. **64:**497–501.
50. **Plump, A. S., L. Erskine, C. Sabatier, K. Brose, C. J. Epstein, C. S. Goodman, C. A. Mason, and M. Tessier-Lavigne.** 2002. Slit1 and Slit2 cooperate to prevent premature midline crossing of retinal axons in the mouse visual system. Neuron **33:**219–232.
51. **Puche, A. C., and M. T. Shipley.** 1999. Odor-induced, activity-dependent transneuronal gene induction in vitro: mediation by NMDA receptors. J. Neurosci. **19:**1359–1370.
52. **Schmetsdorf, S., U. Gartner, and T. Arendt.** 2005. Expression of cell cycle-related proteins in developing and adult mouse hippocampus. Int. J. Dev. Neurosci. **23:**101–112.
53. **Segre, J. A., C. Bauer, and E. Fuchs.** 1999. Klf4 is a transcription factor required for establishing the barrier function of the skin. Nat. Genet. **22:**356–360.
54. **Shindo, T., I. Manabe, Y. Fukushima, K. Tobe, K. Aizawa, S. Miyamoto, K. Kawai-Kowase, N. Moriyama, Y. Imai, H. Kawakami, H. Nishimatsu, T. Ishikawa, T. Suzuki, H. Morita, K. Maemura, M. Sata, Y. Hirata, M. Komukai, H. Kagechika, T. Kadowaki, M. Kurabayashi, and R. Nagai.** 2002. Kruppel-like zinc-finger transcription factor KLF5/BTEB2 is a target for angiotensin II signaling and an essential regulator of cardiovascular remodeling. Nat. Med. **8:**856–863.
55. **Simmen, R. C., R. R. Eason, J. R. McQuown, A. L. Linz, T. J. Kang, L. Chatman, Jr., S. R. Till, Y. Fujii-Kuriyama, F. A. Simmen, and S. P. Oh.** 2004. Subfertility, uterine hypoplasia, and partial progesterone resistance in mice lacking the Kruppel-like factor 9/basic transcription element-binding protein-1 (Bteb1) gene. J. Biol. Chem. **279:**29286–29294.
56. **Smaldone, S., F. Laub, C. Else, C. Dragomir, and F. Ramirez.** 2004. Identification of MoKA, a novel F-box protein that modulates Kruppel-like transcription factor 7 activity. Mol. Cell. Biol. **24:**1058–1069.
57. **Tanaka, H., T. Yamashita, M. Asada, S. Mizutani, H. Yoshikawa, and M. Tohyama.** 2002. Cytoplasmic p21(Cip1/WAF1) regulates neurite remodeling by inhibiting Rho-kinase activity. J. Cell Biol. **158:**321–329.
58. **Tanaka, H., T. Yamashita, K. Yachi, T. Fujiwara, H. Yoshikawa, and M. Tohyama.** 2004. Cytoplasmic p21(Cip1/WAF1) enhances axonal regeneration and functional recovery after spinal cord injury in rats. Neuroscience **127:**155–164.
59. **Theil, T., G. Alvarez-Bolado, A. Walter, and U. Ruther.** 1999. Gli3 is required for Emx gene expression during dorsal telencephalon development. Development **126:**3561–3571.
60. **van Lookeren Campagne, M., and R. Gill.** 1998. Tumor-suppressor p53 is expressed in proliferating and newly formed neurons of the embryonic and postnatal rat brain: comparison with expression of the cell cycle regulators $p21^{Waf1/Cip1}$, $p27^{Kip1}$, $p57^{Kip2}$, $p16^{Ink4a}$, cyclin G1, and the proto-oncogene Bax. J. Comp. Neurol. **397:**181–198.

61. **Wani, M. A., S. E. Wert, and J. B. Lingrel.** 1999. Lung Kruppel-like factor, a zinc finger transcription factor, is essential for normal lung development. J. Biol. Chem. **274:**21180–21185.
62. **Yokoo, T., H. Toyoshima, M. Miura, Y. Wang, K. T. Iida, H. Suzuki, H. Sone, H. Shimano, T. Gotoda, S. Nishimori, K. Tanaka, and N. Yamada.** 2003. $p57^{Kip2}$ regulates actin dynamics by binding and translocating LIM-kinase 1 to the nucleus. J. Biol. Chem. **278:**52919–52923.
63. **Yoshida, M., Y. Suda, I. Matsuo, N. Miyamoto, N. Takeda, S. Kuratani, and S. Aizawa.** 1997. Emx1 and Emx2 functions in development of dorsal telencephalon. Development **124:**101–111.
64. **Zhou, C., Y. Qiu, F. A. Pereira, M. C. Crair, S. Y. Tsai, and M. J. Tsai.** 1999. The nuclear orphan receptor COUP-TFI is required for differentiation of subplate neurons and guidance of thalamocortical axons. Neuron **24:**847–859.